

Transverse Stiffness Analysis of the Shaft System in the Drive Mechanism of Mobile-Head Spiral Winding Equipment

Yanqi Li, Qifan Zhang*, Gang Chen

College of Mechanical Engineering, Tianjin University of Science & Technology, Tianjin 300222, China

*Correspondence Author

Abstract: *In the field of trenchless mechanical equipment, the mobile-head spiral winding device plays a vital role. Compared with other pipeline rehabilitation technologies, the mobile-head spiral winding repair technique offers high compressive strength, efficient construction, long-distance operation, and the capability for underwater installation. It is particularly suitable for the rehabilitation of large-diameter and non-circular pipelines. To address the issues of main shaft bending and bearing crushing encountered during the operation of the driving system in mobile trenchless spiral winding pipeline rehabilitation equipment, a transverse stiffness model of the shaft system considering bearing stiffness was established based on an analysis of its topological structure. The effectiveness of the modeling approach was validated using finite element simulation techniques. A qualitative analysis of the shaft system's flexibility was conducted with the inclusion of bearing factors. In the modeling process, the integral method was employed to analyze the shaft system stiffness with consideration of bearing stiffness. This provides preliminary theoretical support and essential technical preparation for the subsequent dynamic modeling of the entire machine.*

Keywords: Trenchless spiral winding equipment, Shaft system lateral stiffness model, Finite element simulation.

1. Introduction

The core concept of trenchless pipeline rehabilitation technology is to fix an internal lining pipe to the inner wall of a defective existing pipeline through minimal or no excavation [1]. This forms a composite pipeline structure, enabling the liner and the original pipe to jointly bear various external loads, such as overburden, surface loads, and hydrostatic pressure [2-3]. This approach effectively extends the service life of aging pipelines and provides a reliable solution for buried drainage systems, ensuring their long-term, stable, and safe operation [4-5].

Currently, the most widely used pipeline rehabilitation technologies both domestically and internationally include Cured-in-Place Pipe (CIPP), spiral winding, fold-and-form lining, sliplining, and pipe bursting methods [6].

In the 1990s, the mechanically extruded spiral winding rehabilitation technology was invented and initially applied by Australians, and was later acquired by a Japanese company. Around the year 2000, this technique was introduced into

China and was first promoted and implemented in the eastern coastal regions [7]. The basic principle involves a hydraulic power station located on the ground supplying power to the winding machine underground via oil transmission lines. The machine head drives the coiled profile to continuously form a new pipe through spiral winding, followed by grouting and other operations to complete the rehabilitation process. The mechanically extruded spiral winding pipeline rehabilitation equipment offers several advantages, including high compressive strength of the formed pipe, fast construction speed, extended continuous operation distance, the ability to work under water, and suitability for rehabilitating large-diameter and non-circular pipelines. It has now been widely applied in trenchless rehabilitation projects for non-standard pipelines [8]. During the mobile-head spiral winding process, the winding machine advances inside the pipeline as the liner is continuously formed by spiral winding, as shown in Figure 1. The mobile spiral winding equipment demonstrates greater adaptability to various pipeline conditions and a broader range of applications, representing a cutting-edge technology in the field of trenchless pipeline rehabilitation [9].

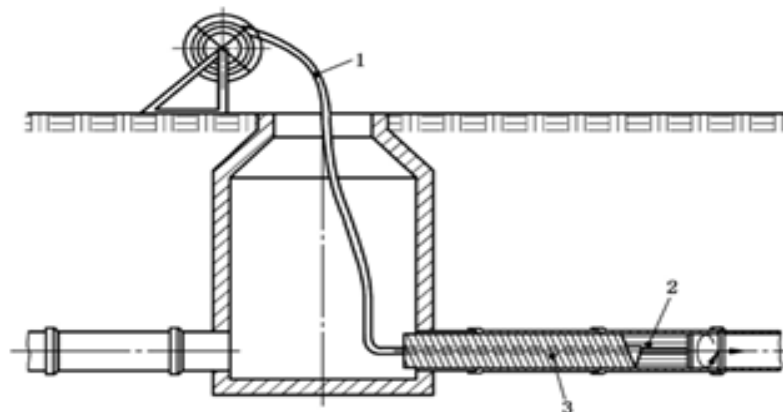
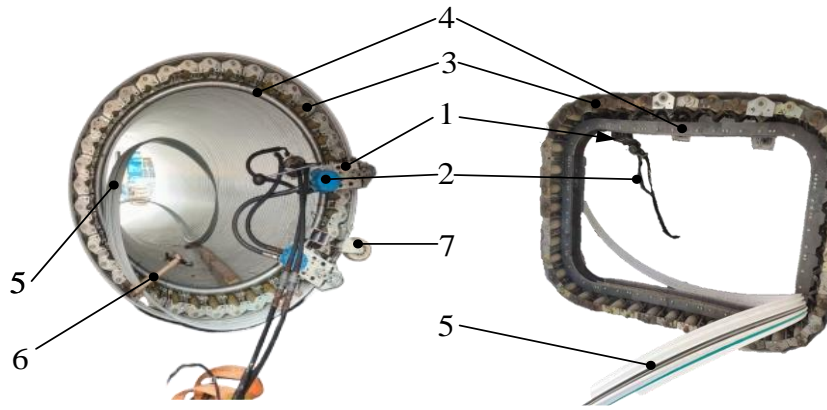


Figure 1: Schematic Diagram of Mobile-Head Spiral Winding



1. Driving Head (Drive System), 2. Hydraulic System, 3. Chain Roller Support Frame, 4. Forming Frame, 5. Profile, 6. Feeding Frame, 7. Driving Wheels
Figure 2: Structural Components of the Spiral Winding Equipment

However, due to the highly complex conditions of urban underground pipeline networks in China, the equipment faces a significant risk of structural failure when operating in complex pipeline sections. When the device traverses areas with abrupt changes in pipe cross-section—such as sharp bends or diameter transitions—the instantaneous resistance peak can reach 4 to 6 times the value under normal operating conditions [10]. This far exceeds the designed load-bearing capacity of the main shaft in the drive system, resulting in plastic bending failure of the shaft. Therefore, in response to the technical challenges arising from the increasing complexity of the topological structure of urban underground pipeline networks in China, this study focuses on the key failure modes of mobile-head spiral winding pipeline rehabilitation equipment under constraints of unstructured underground spaces [11-12]. Specifically, during dynamic construction processes, issues such as elastic buckling deformation of the rubber roller main shaft on the machine frame under asymmetric loads, and failure of deep groove ball bearings—such as cage fracture and raceway collapse—under cyclic impact loads have been observed. These problems significantly affect the quality of the formed liner, thereby compromising both construction efficiency and overall repair quality [13-14].

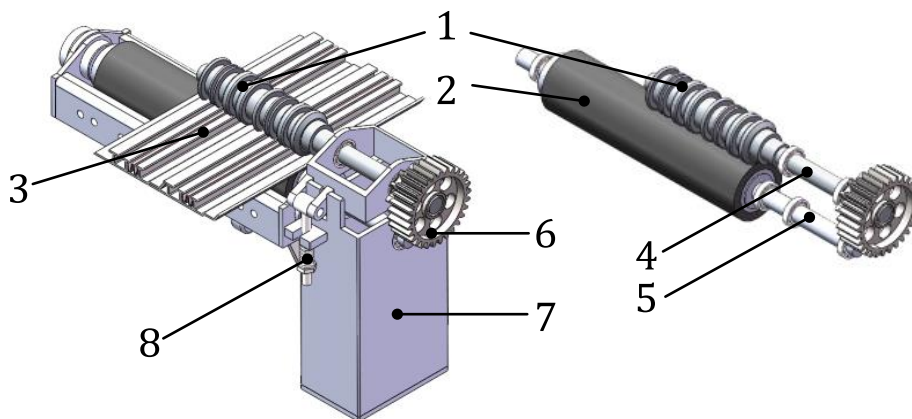
To address the aforementioned issues, this study proposes a transverse stiffness modeling method applicable to the shaft system of such powered head mechanisms [15]. First, the integral method is employed to derive the shaft deflection

coefficients. Then, the effect of bearing stiffness is simplified based on the actual support conditions of the shaft system. Next, the topological relationship between bearing positions and deflection points is considered to complete the stiffness model. Finally, the effectiveness of the proposed model is validated through finite element simulation [16-17].

2. Drive System Design of the Mobile Spiral Winding Equipment

2.1 Structural Components

The mechanism consists of a machine frame, pressure rollers, powered rubber rollers, and traveling wheels. Its main function is to correctly press-fit the profile and ensure the entire machine advances smoothly. Inside the machine frame, a three-stage fixed-axis transmission gear set is installed, which guarantees a profile winding speed of 8 to 12 m/min. On the sides of the machine frame, lifting guide rails are mounted; the upper and lower frames are connected by compression springs. These two devices together ensure the smoothness of the profile winding process. The pressure rollers and powered rubber rollers function to securely engage the male and female locks of the profile and to facilitate the spiral winding of the liner pipe for rehabilitation. The structure of the machine head and the shaft system are shown in Figure 3.



1. Pressure Roller, 2. Powered Rubber Roller, 3. Profile, 4. Pressure Roller Shaft, 5. Rubber Roller Shaft, 6. Traveling Wheel, 7. Machine Frame, 8. Spring
Figure 3: Machine Head and Shaft System Model

Profile: The profile is composed of PVC-U strips, galvanized steel bands, and sealing strips. The outer surface of the profile is covered with T-shaped ribs to enhance its structural strength, while the inner wall is smooth and flat to improve hydraulic flow characteristics. Additionally, the profile features a male-female locking mechanism that, under the compression of the pressure roller and rubber roller, enables the formation of a spirally wound liner pipe.

Traveling Wheels: The traveling wheels are installed at the four corners and the middle of the horizontal plane of the support frame. Designed as adjustable components, they help reduce part of the forming frame's weight. During axial movement, the wheels maintain the balance of the forming frame and prevent it from tipping over, thereby reducing frictional resistance during the winding process.

Spring: The spring connects the upper and lower machine

frames and serves to mitigate impact loads on the main shaft under extreme operating conditions. It is fixed to the upper and lower frames by bolts and nuts. By adjusting the bolt tightening depth, the spring's preload can be controlled, effectively reducing the impact load experienced by the main shaft.

2.2 Operating Principle

The hydraulic motor drives the transmission gears inside the main shaft box, causing the powered rubber roller and the pressure roller to rotate about fixed axes, thereby pressing and locking the profile. The compression spring between the upper and lower machine frames limits the opening angle between them, ensuring the quality of the profile forming process and mitigating impact loads on the main shaft under extreme operating conditions. The topological structure of the equipment is shown in Figure 4.

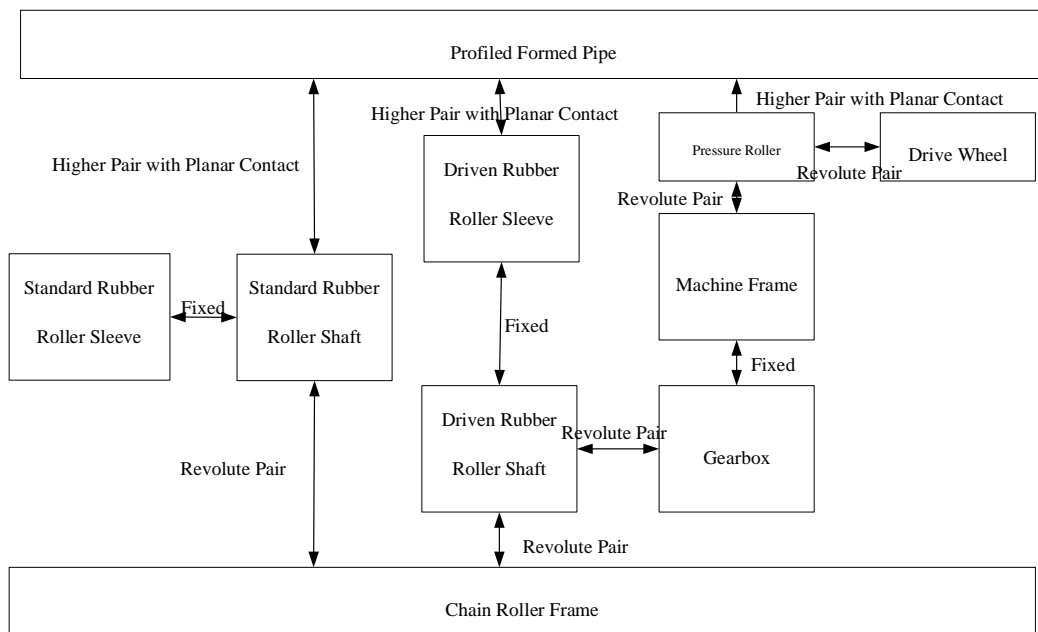


Figure 4: Equipment Topology Diagram

Under extreme operating conditions, the equipment may experience main shaft bending and bearing crushing failures. The shaft system, which supports the primary transmission components, has stiffness closely related to the equipment's operational stability under such conditions. In the following, an appropriate simplification of the shaft system is presented. Using the integral method, a transverse stiffness calculation approach is proposed that considers the concentrated masses of the pressure rollers, rubber rollers, traveling wheels, and the machine frame.

3. Modeling of the Shaft System Transverse Stiffness

The rubber roller shaft and pressure roller shaft are simplified and modeled as shafts with uniform bending stiffness, taking the minimum diameter of each shaft segment as the equivalent diameter. To avoid excessive mathematical complexity, the following additional assumptions are made:

(1) The axial displacement of the rubber roller shaft and pressure roller shaft along their own axes is neglected.

(2) The coupling between the generalized coordinates of torsional displacement and linear displacement is neglected.

To calculate the stiffness influence coefficients at the locations of the concentrated masses, the bearings at each point are initially assumed to be rigid. The pressure roller shaft and rubber roller shaft system are modeled as cantilever beams. The corresponding transverse stiffness model is illustrated in Figures 5 and 6. Here, m_1 , m_2 , m_3 , and m_4 represent the concentrated masses of the traveling wheel, pressure roller, machine frame, and powered rubber roller, respectively, while points A, B, C, and D denote the four bearings in the two shaft systems.

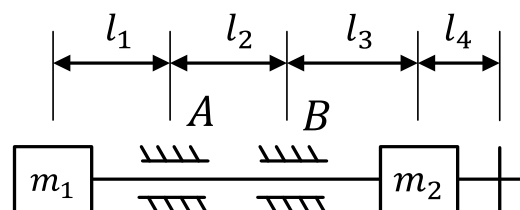


Figure 5: Transverse Stiffness Model of the Pressure Roller Shaft System

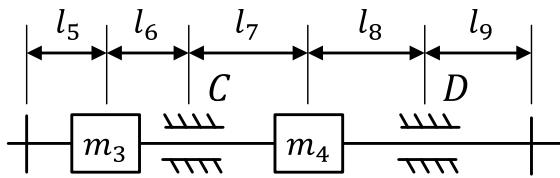


Figure 6: Transverse Stiffness Model of the Rubber Roller Shaft System

As shown in the figures, the pressure roller shaft system is supported by two bearings, A and B, while the rubber roller shaft system is supported by bearings C and D. When external forces are applied to the shaft systems, the support reactions at the bearings are determined using static equilibrium equations. The shaft deflections at the locations of the concentrated masses are then calculated accordingly.

3.1 Flexibility Coefficient of the Shaft System

In the stiffness modeling process, the support reactions at the bearings must be determined prior to calculating the transverse stiffness coefficients at the locations of the concentrated masses. The force method is employed by applying a unit force P at each concentrated mass location to establish the static equilibrium model. The shaft system flexibility model is then formulated and calculated using the integral method.

(1) When a unit force is applied at the positions of the pressure roller and traveling wheel, the constraints imposed by bearings A and B on the shaft system are replaced with support reactions FP according to the force method. Based on this approach, a new static equilibrium system is established, as illustrated in Figure 7.

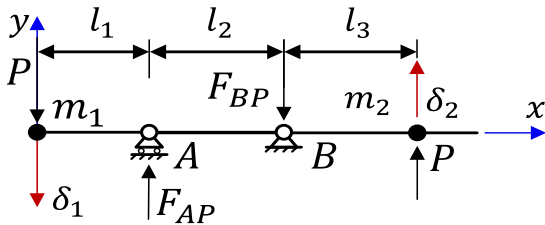


Figure 7: Support Reaction Model of the Pressure Roller Shaft System

When a unit force is applied at the positions of the pressure roller and traveling wheel, the constraints imposed by bearings A and B on the shaft system are replaced with support reactions FP according to the force method. Based on this approach, a new static equilibrium system is established, as illustrated in Figure 7.

The symbols in the figure are defined as follows: P represents the unit force applied at the positions of the traveling wheel and pressure roller; F_{AP} and F_{BP} denote the support reactions at the simply supported points A and B, respectively; l_1 is the distance between the concentrated mass m_1 and support point A; l_2 is the distance between support points A and B; l_3 is the distance from support point B to the concentrated mass m_2 .

The deflections at the concentrated mass points m_1 and m_2

under the action of unit force P applied to the shaft system are calculated, as illustrated in Figure 8.

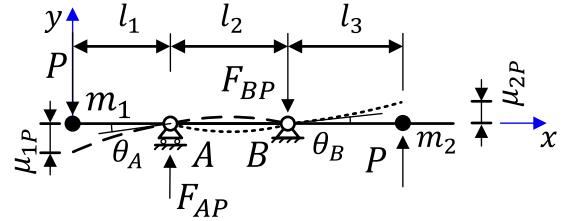


Figure 8: Deflection Model of the Pressure Roller Shaft System under Unit Force P

According to the principles of mechanics of materials, the angular displacement (rotation) at point A under the action of force P on segment AB is given by:

$$\theta_A = -\frac{Pl_1l_2}{3EI} \quad (1)$$

In the equation, M_P denotes the bending moment generated by the force P at point A:

$$M_P = Pl_1 \quad (2)$$

Under the action of force P, the deflection at point m_1 is given by:

$$\mu_{1P} = -\frac{Pl_1^2}{3EI}(l_1 + l_2) \quad (3)$$

Under the action of force P, the deflection at point m_2 is given by:

$$\mu_{2P} = -\frac{Pl_3^2}{3EI}(l_2 + l_3) \quad (4)$$

(2) When a unit force is applied at the positions of the driving rubber roller and the frame, the constraints imposed by bearings C and D on the shaft system are replaced by support reactions FP according to the force method. A new force equilibrium system is then established, as illustrated in Figure 9.

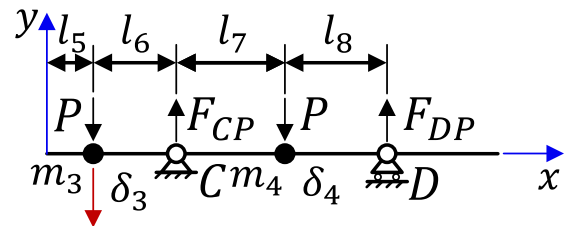


Figure 9: Support Reaction Model of the Rubber Roller Shaft System

The meanings of the symbols in the figure are as follows: P is the unit force applied at the position of the walking wheel. F_{CP} and F_{DP} represent the support reactions at bearing supports C and D, respectively. l_5 is the distance from the left end of the shaft to the concentrated mass m_3 , l_6 is the distance from the concentrated mass m_3 to support point C. l_7 is the distance from support point D to the concentrated mass m_4 . l_8 is the distance from the concentrated mass m_4 to support point D.

The deflections at the concentrated mass points m_3 and m_4 under the action of unit force P applied to the shaft system are calculated, as illustrated in Figure 10.

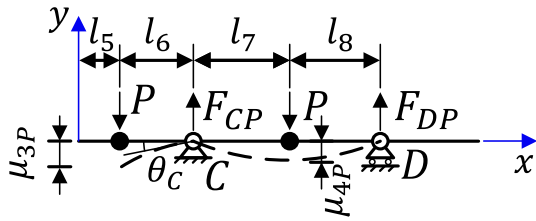


Figure 10: Deflection Model of the Rubber Roller Shaft System Under Unit Force P

According to the principles of mechanics of materials, the rotation angle at point C under the action of force P in the segment m_4C is given by:

$$\theta_C = -\frac{Pl_6l_7}{3EI} \quad (5)$$

The deflection at point m_3 under the action of force P is:

$$\mu_{3P} = -\frac{Pl_6^2}{3EI}(l_6 + l_7) \quad (6)$$

When forces F_1 and F_2 act at the concentrated mass points m_1 and m_2 , respectively, the deflection equation for segment m_1A is:

$$\mu_{m_1A} = \frac{1}{6EI}(-F_1x^3 + C_1x + C_2) \quad (7)$$

The deflection equation for segment AB is:

$$\mu_{AB} = \frac{1}{6EI}(-F_1x^3 + F_{AP}(x - l_1)^3 + C_3x + C_4) \quad (8)$$

The deflection equation for segment Bm_2 is:

$$\mu_{Bm_2} = \frac{1}{6EI}(-F_1x^3 + F_{AP}(x - l_1)^3 + F_{BP}(x - l_1 - l_2)^3 + C_5x + C_6) \quad (9)$$

The deflection equation for the segment from m_2 to the right end is:

$$\mu_{m_2} = \frac{1}{6EI} \left(-F_1x^3 + F_{AP}(x - l_1)^3 + F_{BP}(x - l_1 - l_2)^3 + F_2(x - l_1 - l_2 - l_3)^3 + C_7x + C_8 \right) \quad (10)$$

When force F acts at the concentrated mass points m_3 and m_4 , the deflection equation for the segment from the left end to m_3 is:

$$\mu_{m_3} = \frac{1}{6EI}(F_1x^3 + C_1x + C_2) \quad (11)$$

The deflection equation for segment m_3C is:

$$\mu_{m_3C} = \frac{1}{6EI}(F_1x^3 - F_{CP}(x - l_4)^3 + C_3x + C_4) \quad (12)$$

The deflection equation for segment Cm_4 is:

$$\mu_{Cm_4} = \frac{1}{6EI}(F_1x^3 - F_{CP}(x - l_4)^3 + F_{DP}(x - l_4 - l_5)^3 + C_5x + C_6) \quad (13)$$

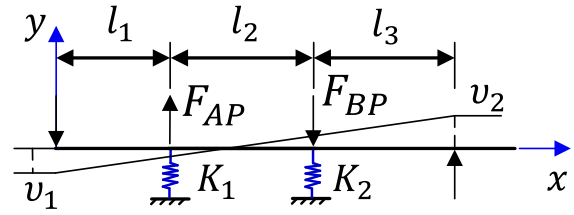
The deflection equation for the segment from m_4 to the right end is:

$$\mu_{m_4} = \frac{1}{6EI} \left(F_1x^3 - F_{CP}(x - l_4)^3 + F_{DP}(x - l_4 - l_5)^3 - F_2(x - l_4 - l_5 - l_6)^3 + C_7x + C_8 \right) \quad (14)$$

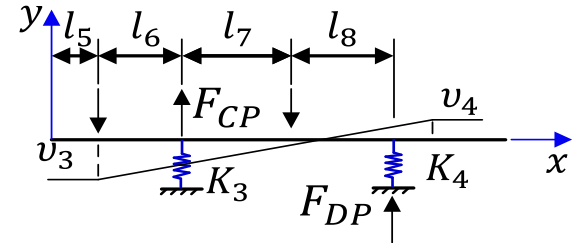
3.2 Shaft System Stiffness Considering Bearing Stiffness

To investigate the bearing deformation and its overall effect on the shaft system deformation, a model of bearing stiffness influence coefficients in the shaft system is established,

considering the bearing stiffness and its positional distribution within the shaft system, as shown in Figure 11.



(a) Pressure Roller Shaft System



(b) Driven Rubber Roller Shaft System

Figure 11: Bearing Stiffness Influence Coefficient Model

The simply supported bearings are modeled as springs with certain stiffness. Here, F_{xp} represent the reaction forces at the four bearings, and μ_i denote the deformation displacements at each bearing, where $x=A,B,C,D$ and $i=1,2,3,4$. The displacement deformation at the bearings is expressed as:

$$\mu_i = \frac{F_x}{K_i} \quad (15)$$

The influence coefficient of bearing deformation on the shaft deflection for segment m_1m_2 is:

$$\mu_{zm_1m_2} = \mu_2 - x \frac{\mu_1 + \mu_2}{l_2} \quad (16)$$

The influence coefficient of bearing deformation on the shaft deflection for segment m_3D is:

$$\mu_{zm_3D} = \mu_3 - x \frac{\mu_3 + \mu_4}{l_6 + l_7} \quad (17)$$

Considering both bearing stiffness and shaft system flexibility, based on the principle of linear superposition for small deformations, the total flexibility can be regarded as the sum of their respective deflections, which can be expressed as:

$$\delta = \mu + \mu_z \quad (18)$$

Thus, the shaft system flexibility model considering bearing stiffness is obtained.

Segment m_1m_2 :

$$\mu_{m_1m_2} = \frac{1}{6EI} \left(-F_1x^3 + F_{AP}(x - l_1)^3 + F_{BP}(x - l_1 - l_2)^3 + C_5x + C_6 \right) + \mu_2 - x \frac{\mu_1 + \mu_2}{l_2} \quad (19)$$

Segment m_3D :

$$\mu_{m_3} = \frac{1}{6EI} \left(F_1x^3 - F_{CP}(x - l_4)^3 + F_{DP}(x - l_4 - l_5)^3 - F_2(x - l_4 - l_5 - l_6)^3 + C_7x + C_8 \right) + \mu_3 - x \frac{\mu_3 + \mu_4}{l_6 + l_7} \quad (20)$$

By substituting the variables in the above flexibility coefficient expressions and applying the parameters at different concentrated mass positions x , and expressing them in matrix form, the transverse stiffness matrix K of the shaft system can be obtained as:

$$K_1 = \begin{bmatrix} \delta_{11} & \delta_{12} \\ \delta_{21} & \delta_{22} \end{bmatrix}^{-1} \quad K_2 = \begin{bmatrix} \delta_{31} & \delta_{32} \\ \delta_{41} & \delta_{42} \end{bmatrix}^{-1} \quad (21)$$

In the equation, δ_{ij} represents the flexibility coefficient corresponding to the respective mass point.

4. Finite Element Simulation

In ANSYS, the shaft system model was established by defining material properties, applying physical constraints, generating the mesh, and refining the local mesh in contact regions.

4.1 Boundary Conditions and Basic Settings

The components are made of 45# steel. The mesh is generated along the X-axis, using the actual bearing locations as reference points. Fixed support constraints are applied at the three bearing positions. A unit force P is sequentially applied at the positions corresponding to the walking wheel (m_1), pressure roller (m_2), housing frame (m_3), and driving rubber roller (m_4).

4.2 Simulation of Flexibility Coefficients

A trajectory line was defined along the shaft centerline to generate the shear force, bending moment, and deflection diagrams. In the Solution module, Total Deformation was selected, and under the Directional Deformation section, the corresponding results were generated. The deformation response of the shaft system under a unit force applied at a specific concentrated mass location was obtained. An example of the deformation result when the unit force is applied at the pressure roller position is shown in Figure 12.

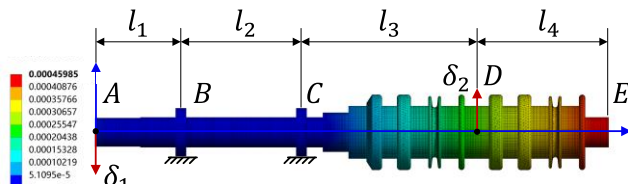


Figure 12: Simulation results of shaft system flexibility when a unit load is applied at the pressure roller.

5. Numerical Example

5.1 Basic Parameters

The basic parameters of the drive system shaft are listed in Table 1. A MATLAB program was developed to calculate the shaft system's flexibility under unit loads applied at the four concentrated mass points: the crawler wheel, the pressing roller, the machine housing, and the driving rubber roller.

Table 1: Basic Parameters of the Driving System Shaft

Name	Value	Name	Value
l_1	56.5 mm	l_8	259.5 mm
l_2	80 mm	l_9	29 mm
l_3	108.5 mm	Young's modulus	206 Gpa
l_4	95 mm	Moment of Inertia	7854 mm ⁴
l_5	53 mm	Bearing stiffness	3.0×10^7 N/m
l_6	82 mm	Bearing Model	61804
l_7	66.5 mm	Equivalent Diameter of Shaft Segment	20 mm

5.2 Theoretical Calculation Results

According to the methods described in Sections 2.1 and 2.2, the flexibility values of the entire shaft system were calculated and organized, as shown in Figures 13 and 14. For clarity, the flexibility values are presented on the vertical axis.

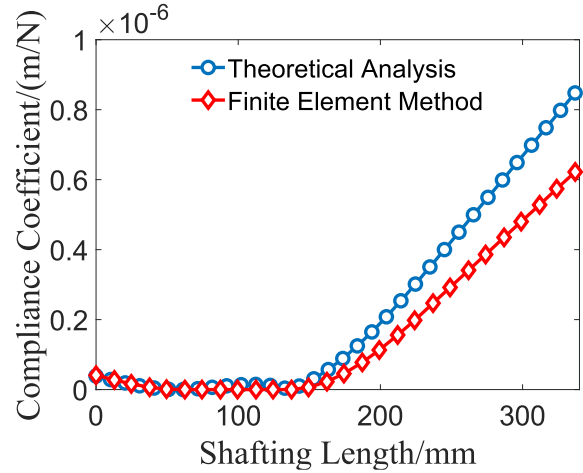


Figure 13: Deflection Flexibility Coefficient of the Pressure Roller

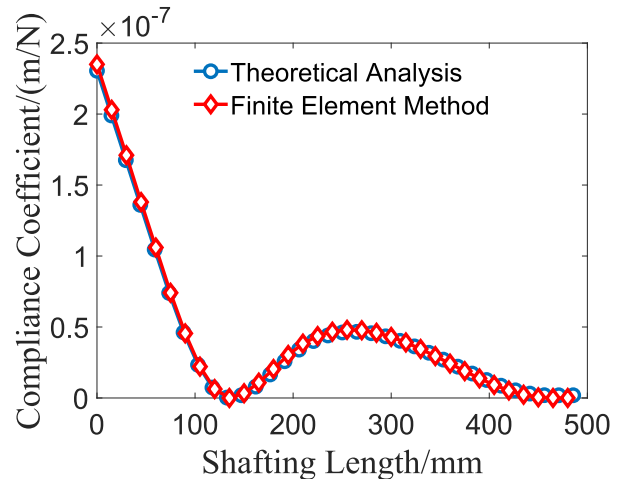


Figure 14: Deflection Flexibility Coefficient of the Rubber Roller

As shown in Figures 13 and 14, the theoretical modeling results and finite element simulation results exhibit consistent trends in the flexibility variation along different positions of the shaft system. This indicates that the developed model can accurately capture the lateral stiffness characteristics of the shaft system to a certain extent.

Additionally, the figures also illustrate the variation of the flexibility coefficients when the concentrated masses are located at different key positions corresponding to the critical dimension parameters l_1 , l_3 , l_5 , and l_7 .

5.3 Effect of Bearing Support Stiffness on Flexibility

By assuming the bearing stiffness at supports A, B, C, and D to be infinitely large, a qualitative simulation analysis was conducted to investigate the influence of the stiffness of these bearing supports on the overall flexibility of the shaft system. The results are shown in Figures 15 and 16.

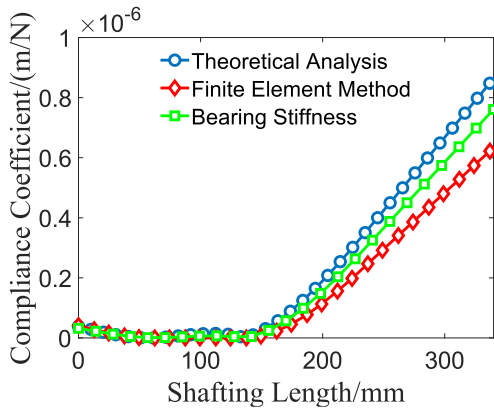


Figure 15: Deflection Flexibility Coefficient of the Pressure Roller

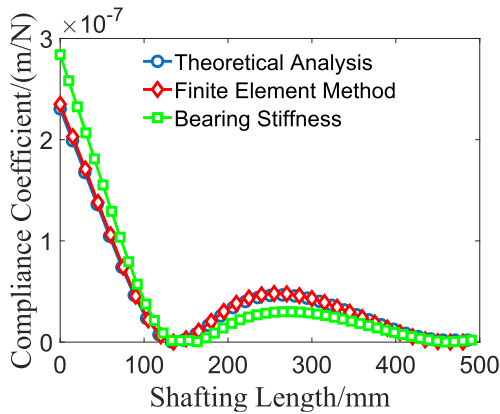


Figure 16: Deflection Flexibility Coefficient of the Rubber Roller

When bearing stiffness is considered, the flexibility at the crawler concentrated mass shows no significant change. The flexibility at the press roller concentrated mass decreases, showing a positive correlation with bearing stiffness. Similarly, the flexibility at the concentrated mass of the driven rubber roller decreases, also exhibiting a positive correlation. However, the flexibility at the concentrated mass of the press roller shaft's gearbox increases, indicating a negative correlation.

By considering the bearing stiffness as a constant, a qualitative analysis was conducted on the influence of the support stiffness of four types of bearings—cylindrical roller bearing, tapered roller bearing, angular contact ball bearing, and deep groove ball bearing—on the shaft system flexibility under identical dimensions. The results are shown in Figures 17 and 18.

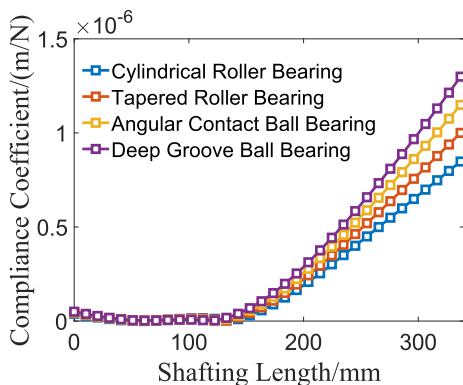


Figure 17: Deflection Flexibility Coefficient of the Pressure Roller

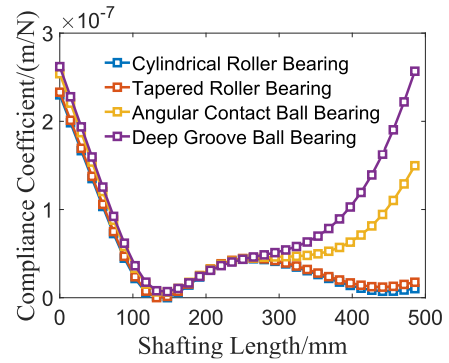


Figure 18: Deflection Flexibility Coefficient of the Rubber Roller

As shown in the figures, the stiffness of the support bearings at various locations has a significant and complex impact on the overall shaft system flexibility. Among the four types of bearings, the cylindrical roller bearing exhibits the highest support stiffness and the lowest shaft system flexibility. This indicates that, for the shaft system mechanism of the mechanical spiral winding pipeline repair equipment drive system, increasing the bearing stiffness is effective in reducing the flexibility of both the pressure roller shaft and the rubber roller shaft.

By comparing the lateral vibration stiffness model of the shaft system established in this study, which considers bearing stiffness, with the model that neglects bearing stiffness, it can be observed that the support bearing stiffness at various locations significantly affects the overall shaft system flexibility. Increasing the bearing stiffness has a certain effect in reducing the shaft system flexibility.

6. Conclusions

This paper establishes a lateral stiffness model of the drive shaft system for the walking-type mechanical spiral winding equipment, based on the flexibility coefficient method and the principle of small displacement linear superposition, while incorporating the effect of bearing stiffness.

(1) The comparison between the theoretical model and finite element simulation results shows that both exhibit consistent overall trend patterns, demonstrating that the proposed modeling approach has high reliability.

(2) Bearing support stiffness is one of the key factors influencing the stiffness of the mechanical spiral winding equipment drive system, and its magnitude has a significant and complex impact on the dynamic characteristics of the drive system.

(3) By analyzing the effect of support stiffness of different types of bearings on the shaft system flexibility, it is evident that bearing stiffness significantly influences the overall shaft system flexibility; increasing the bearing support stiffness can effectively reduce the shaft flexibility at each concentrated mass location.

References

[1] Zhou L, Zhao J Y, Yang X Y, et al. Study on Optimal Selection of Trenchless Rehabilitation Technologies for

Yanqi Li (1971—), male, Native of Heilongjiang Province, Professor. E-mail: lyqjj@tust.edu.cn

- Drainage Pipelines Based on Analytic Hierarchy Process [J]. *Water Supply and Drainage*, 2015, 51(03): 94-97.
- [2] Wang H P, An G F, Xie G Y. Interpretation of “Technical Specification for Inspection and Evaluation of Urban Drainage Pipelines” (CJJ181-2012) [J]. *Water Supply and Drainage*, 2014, 50(02): 124-127.
- [3] Sun Y P. Trenchless Rehabilitation Technology for Underground Pipelines in Japan [J]. *Urban Management Technology*, 2008: 62-63.
- [4] Ma B S. *Trenchless Engineering* [M]. Beijing: People's Transportation Publishing House, 2008.
- [5] Zhou S C, Yang Y H, Shen Y, et al. Dynamic Modeling and Optimal Design of a Novel Indexing Mechanism [J]. *Journal of Mechanical Engineering*, 2010, 46(19): 9-16.
- [6] Chang Z Y, Zhang C, Yang Y H, et al. Dynamic Modeling of a Cam Indexing Mechanism with Curved Surface Based on Kane's Equations [J]. *Journal of Mechanical Engineering*, 2001(03): 34-37+40.
- [7] Tang Jianguo, Zhu Baoluo. Classification and Selection of Trenchless Repair Technologies for Drainage Pipelines [J]. *Water Supply and Drainage*, 2005(06): 83-90.
- [8] Lin, Jinfeng. Application of Trenchless Spiral Winding Rehabilitation Technology in Drainage Pipeline Repair Projects [J]. *Construction Science and Technology*, 2023, 22(19): 85-87.
- [9] Shen, Yu, Yang, Yuhu, Zhang, Ce, et al. Dynamic Analysis of Cam Indexing Mechanism with Clearance [J]. *Mechanical Science and Technology*, 2001(05): 714-715+725-734.
- [10] Kuang J H, Lin A D, Ho T Y, Dynamic responses of a globoidal cam system, *ASME Journal of Mechanical Design*, 2004, 126(5): 909-915.
- [11] Incerti G, Dynamic modelling of cam indexers driven by DC servomotors, *Proceedings of the 2006 IEEE International Conference on Control Applications*, Munich, Germany, 2008, 1392-1397.
- [12] Sun X Q, Yang Y H, Liu N, et al, Study on dynamics modeling and analysis of parallel indexing cam system, *Proceeding of the 2004 the Eleventh World Congress in Mechanism and Machine Science*, Tianjin, China, 2004, 1040-1043.
- [13] Mao L H. Application of the Lining Turnover Repair Technique of Cipp Hoses [J]. *Shanxi Architecture*, 2008(14): 112-113.
- [14] Chang, Zongyu, Zhang, Ce, Yang, Yuhu, et al. Dynamic Modeling of Arc-Surface Indexing Cam Mechanism Using Kane's Equations [J]. *Journal of Mechanical Engineering*, 2001, 37(3): 34-40.
- [15] Zhang, Ce, Liu, Mingtao, Yang, Yuhu, et al. Design and Simulation of a Novel Planetary Indexing Cam Profile [J]. *Journal of Tianjin University*, 2006(01): 100-103.
- [16] Shan, Peng, Liu, Mingtao, Chen, Gang, et al. Analysis of the Inherent Characteristics of a Double-Engagement Indexing Mechanism [J]. *Mechanical Design*, 2022, 39(09): 46-52.
- [17] Xu, Fuwei, Fu, Rong, Fan, Jianhui, et al. *Mechanics of Materials* [M]. Nanjing: Southeast University Press, 2017, 08.249.

Author Profile